Acta Pharmaceutica Sinica B 2022;12(8):3410–3426

Chinese Pharmaceutical Association
Institute of Materia Medica, Chinese Academy of Medical Sciences

Acta Pharmaceutica Sinica B

www.elsevier.com/locate/apsb
www.sciencedirect.com

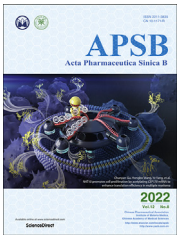

ORIGINAL ARTICLE

Membrane-camouflaged supramolecular nanoparticles for co-delivery of chemotherapeutic and molecular-targeted drugs with siRNA against patient-derived pancreatic carcinoma

Honglin Tang[a,b,†], Yanan Xue[a,b,†], Bowen Li[b,*], Xiaojie Xu[b], Fu Zhang[a,c], Jiajing Guo[b], Qijun Li[a], Tingting Yuan[b], Yuan Chen[b], Yubin Pan[a], Yuan Ping[b,*], Da Li[a,*]

[a]*Department of Medical Oncology, Sir Run Run Shaw Hospital, School of Medicine, Zhejiang University, Hangzhou 310058, China*
[b]*College of Pharmaceutical Sciences, Zhejiang University, Hangzhou 310058, China*
[c]*Department of Hepatobiliary and Pancreatic Surgery, the First Affiliated Hospital, Zhejiang University, Hangzhou 310003, China*

Received 24 October 2021; received in revised form 16 January 2022; accepted 18 January 2022

KEY WORDS

Chemotherapy;
Target therapy;
siRNA;
Nanomedicine;
Hybrid membrane;
Drug antagonism;
Pancreatic carcinoma;
Patient-derived tumor

Abstract Pancreatic cancer remains one of the most lethal malignancies worldwide. The combination of the first-line standard agent gemcitabine (GEM) with the molecular-targeted drug erlotinib (Er) has emerged as a promising strategy for pancreatic cancer treatment. However, the clinical benefit from this combination is still far from satisfactory due to the unfavorable drug antagonism and the fibrotic tumor microenvironment. Herein, we propose a membrane-camouflaged dual stimuli-responsive delivery system for the co-delivery of GEM and Er into pancreatic cancer cells and tissues to block the antagonism, as well as reshapes profibrotic tumor microenvironment *via* simultaneous delivery of small interference RNA (siRNA) for synergistic pancreatic cancer treatment. This "all-in-one" delivery system exhibits sensitive GSH and pH-dependent drug release profiles and enhances the inhibitory effects on the proliferation and migration of tumor cells *in vitro*. Excitingly, the systemic injection of such a biomimetic drug co-delivery system not only resulted in superior inhibitory effects against

*Corresponding authors.
E-mail addresses: bowen_li@zju.edu.cn (Bowen Li), pingy@zju.edu.cn (Yuan Ping), lidaonconew@zju.edu.cn (Da Li).
[†]These authors made equal contributions to this work.
Peer review under responsibility of Chinese Pharmaceutical Association and Institute of Materia Medica, Chinese Academy of Medical Sciences.

https://doi.org/10.1016/j.apsb.2022.02.007

orthotopic pancreatic tumor and patient-derived tumor (PDX), but also greatly extended the survival rate of tumor-bearing mice. Our findings provide a promising therapeutic strategy against pancreatic cancer through the enhanced synergistic effect of target therapy, chemotherapy and anti-fibrotic therapy, which represents an appealing way for pancreatic cancer treatment.

1. Introduction

Pancreatic cancer remains one of the leading causes of cancer-related death worldwide[1]. Due to the lack of early symptoms, around 80% of patients are diagnosed with locally advanced or metastatic disease rendering them inoperable[2,3]. For decades, gemcitabine (GEM), which functions as nucleoside anticancer drug, has been recommended as the standard of care for palliative and adjuvant treatment in patients with advanced pancreatic cancer[4], yet limited success has been achieved in prolonging the overall survival of patients by GEM monotherapy[5,6]. In recent years, the clinical trials combining GEM with other therapeutic agents including molecular targeted drugs are conducted in an attempt to provide more effective treatments[7,8]. Among the molecular targeted drugs, epidermal growth factor receptor (EGFR) tyrosine-kinase inhibitor has been regarded as one of the most promising drugs for pancreatic cancer therapy. Several researches indicate that the inhibition of EGFR signaling is closely related to reduced pancreatic cancer growth and improved patient prognosis[9,10]. As a result, Erlotinib (Er), a small molecular EGFR inhibitor, has already been approved in combination with GEM as first-line therapy for pancreatic cancer based on the results of increased survival of 10 days in the pivotal phase III of clinical trial[11]. Furthermore, the most recent National Comprehensive Cancer Network (NCCN) Clinical Practice Guideline has recommended GEM-Er combination therapy as a treatment option for pancreatic cancer patients with locally advanced or metastatic disease and good performance status[12]. Although the combination strategy exhibits the advantages of significant clinical survival over GEM alone, for most patients, however, the impact of clinical benefits appears to be modest[11,13]. Therefore, deciphering and blocking the mechanisms responsible for the limited clinical efficacy may shed lights on expanding the benefit of this combination.

The unfavorable antagonism between the tyrosine-kinase inhibitor and nucleoside chemotherapy drug is considered as one of the crucial mechanisms to compromise the efficacy of their combination[14−17]. It is reported that Er inhibits human equilibrative nucleoside transporter 1 (hENT1) necessary for the transportation of nucleoside drugs, resulting in the lowered intracellular accumulation of cytotoxic GEM metabolites[14]. Meanwhile, GEM induces EGFR ligand expression and ERBB2 activation by increasing heterodimer formation with EGFR, thereby offsetting the antitumor effects of Er[16]. Although multiple strategies have been proposed to minimize the antagonism between the two drugs, the therapeutic effect is still far from satisfactory[18,19], suggesting that the failure may also attribute to other factors. Most notably, pancreatic cancer is characterized by the development of extensive fibrosis with stromal components outnumbering cancer cells[20−22]. Abundant evidence suggests that the stromal components play important roles in the chemotherapy and target therapy resistance by activating signaling pathways that limit the therapeutic effects and acting as a mechanical barrier to drug delivery[23−26]. Various therapeutic strategies have been developed, specifically targeting profibrotic pathways involved in tumor desmoplasia to control tumor growth and increase the antitumor effects of chemotherapeutics or target therapies[27−30]. Recent studies identify tumor-stroma IL1β-IRAK4 feedforward circuitry as a key mechanism that drives tumor fibrosis, chemoresistance, and poor prognosis in pancreatic cancer[31,32]. Pharmacologic blockade or silencing of IRAK4 potently suppresses NF-κB activity, which undermines the fibroblast barrier and abolishes the tumorigenic potential of human and murine pancreatic cancer cells, and therefore greatly sensitized pancreatic cancer to various therapies[31,32]. These results highlight IRAK4 blockade as a powerful weapon to deactivate fibroblasts and eliminate stroma, suggesting IRAK4 blockade as complementary therapeutic strategy for the synergism of GEM and Er. Nevertheless, it remains a great challenge to develop a functionalized delivery carrier that can deliver combinational therapeutic agents for above purposes.

In the current study, we propose a proof-of-concept study for pancreatic cancer therapy through the combinational delivery of GEM, Er and IRAK4 siRNA (siIRAK4) mediated by cancer cell-macrophage hybrid membrane-coated nanoparticles (NPs) in an attempt to initiate the synergistic effect of targeted molecular therapy and chemotherapy. As shown in Scheme 1, β-cyclodextrin (β-CD) is assembled with low-molecular-weight polyethylenimine (PEI) as a cationic polymer gene vector (PC), followed by conjugating with the chemotherapeutic agents GEM bridged by a GSH-responsive linker (−SS−) to form a polymer prodrug (GEM-SS-PC). This prodrug can encapsulate the molecular targeted drug Er *via* host–guest supramolecular interaction as a co-delivery system (Er@GEM-SS-PC) for the simultaneous delivery of Er and GEM. Er@GEM-SS-PC is further loaded with siIRAK4 to form a nano-drug (siIRAK4/Er@GEM-SS-PC) for attenuating tumor fibrosis and augmenting the synergistic effect of Er and GEM. It has been reported that cancer cell membrane-coated delivery systems possess the same cell adhesion molecules as their source cells, thereby exhibiting cancer cell-specific targeting capability due to the homotypic binding mechanism[33,34]. Meanwhile, the delivery vector coated with the macrophage membrane reserves the proteins like CD45 and CD14, which help them evade from mononuclear phagocyte system (MPS)-mediated clearance[35]. In order to mitigate MPS-mediated clearance during the systemic circulation and enhance the tumor-targeting capability of our designed co-delivery system,

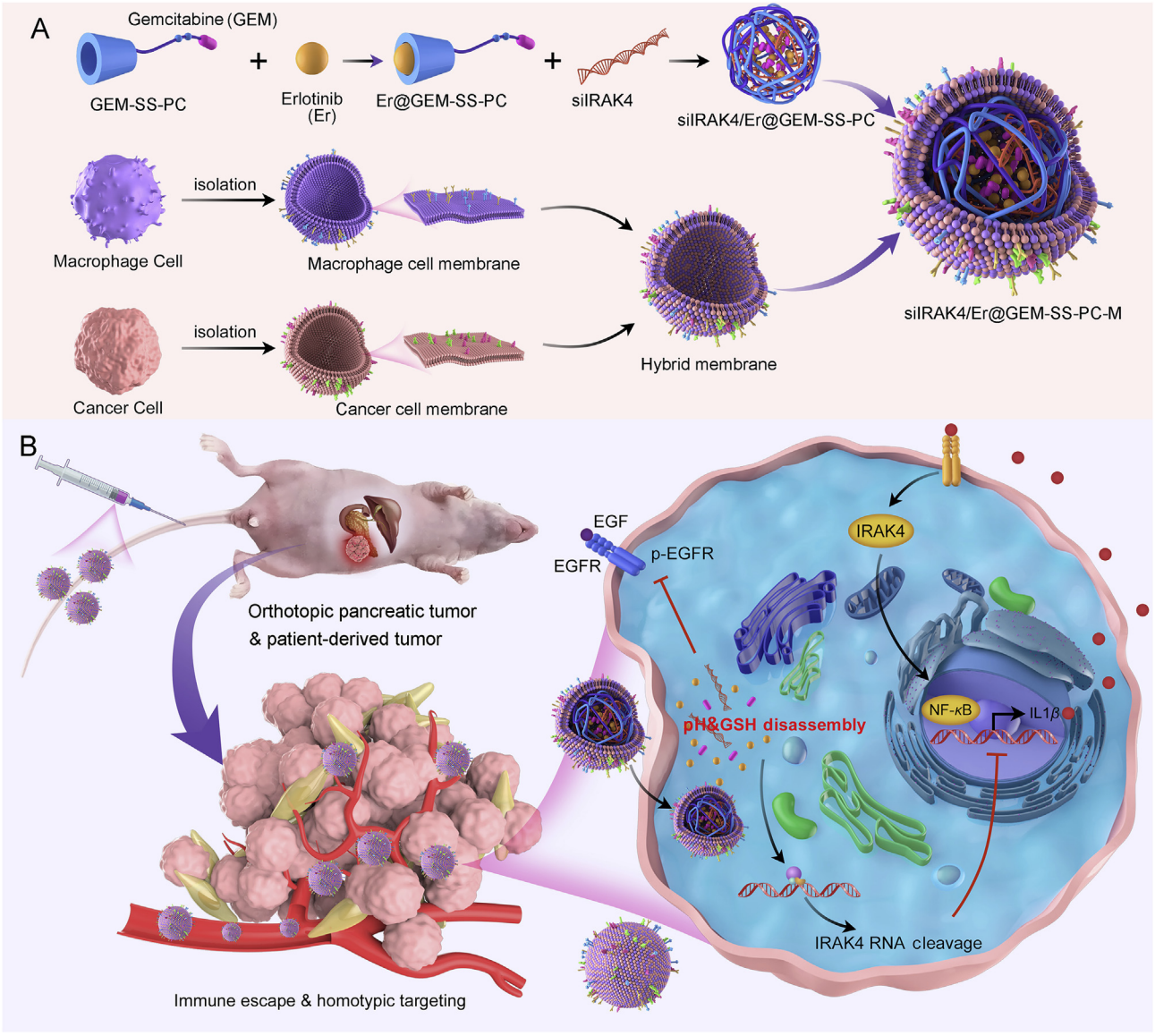

Scheme 1 Construction of cancer cell-macrophage hybrid membrane-coated drug-delivery nanosystem for pancreatic cancer treatment. (A) Schematic illustration for the preparation of siIRAK4/Er@GEM-SS-PC-M: gemcitabine (GEM) is conjugated with PC by a GSH-responsive linker to form GEM prodrug, followed by encapsulating the Erlotinib (Er) *via* host–guest molecular interaction and loading with the siRNA to form cell membrane-coated nano-drug (siIRAK4/Er@GEM-SS-PC-M). (B) Schematic illustration of targeted nanoparticles to deliver to GEM, Er and siIRAK4 against pancreatic tumors including orthotopic pancreatic tumor and patient-derived tumor (PDX).

the related cancer cell-macrophage hybrid membrane reported previously[36] is coated on the siIRAK4/Er@GEM-SS-PC to form a biomimetic nano-drug (siIRAK4/Er@GEM-SS-PC-M). Through the simultaneous co-delivery of GEM, Er and siIRAK4 by the biomimetic nanosystem, we expect to demonstrate that the new therapeutic modality exerts superior anti-stromal activity in the fibrotic tumor microenvironment and blocks the antagonisms between GEM and Er as well, and thereby the combined therapeutic modality is able to cooperatively prolong the overall survival of mice bearing orthotopic pancreatic tumor and patient-derived tumor (PDX). To the best of our knowledge, this is the first study to explore how the combination of anti-stromal therapy, chemotherapy and molecular targeted therapy influences overall antitumor effects through carrier-mediated combinational delivery.

2. Materials and methods

2.1. *Synthesis of PC*

The β-CD (4.20 g, 3.8 mmol) was dissolved in DMSO solution (20 mL), and then added the catalyst CDI (5.00 g, 30.8 mmol). At room temperature, this mixture was stirred for 3 h under N_2, the PEI (MW 600 Da, 18.00 g, 30 mmol) was dissolved in DMSO solution (30 mL) and added dropwise into the above mixture over 3 h under N_2 and then stirred over 24 h. After the completion of the reaction, this mixture was collected and dialyzed against ultrapure water using the dialysis bag for 2 days. The dialyzate was freeze-dried to obtain the white power PC. The chemical structures were determined by ^{1}H NMR.

2.2. Synthesis of disulfanediylbis(ethane-2,1-diyl) bis (4-nitrophenyl) bis(carbonate) (1)

2,2′-Disulfanediylbis (ethan-1-ol) (1.54 g, 10 mmol) and DIPEA (2.58 g, 20 mmol) were dissolved in 50 mL dry DCM under nitrogen atmosphere, and then a mixture of pyridine (1.60 g, 20 mmol) and 4-nitrobenzyl chloroformate (10.75 g, 50 mmol) in 25 mL dry DCM were added dropwise to the above solution at room temperature. After 12 h of reaction, the solvent was removed under reduced pressure, and the mixture was diluted with 100 mL ethyl acetate and washed with 200 mL water. The organic solvent was removed and the crude product was purified by column chromatography on silica gel (DCM:EtOAc 1:1) to obtain compound **1** (4.02; 83%) as a yellow solid. ^{1}H NMR (500 MHz, Chloroform-*d*) δ 8.28 (d, J = 9.2 Hz, 1H), 7.39 (d, J = 9.2 Hz, 1H), 4.58 (t, J = 6.5 Hz, 2H), 3.09 (t, J = 6.5 Hz, 1H).

2.3. Synthesis of 2-((2-(((4-nitrophenoxy)carbonyl)oxy)ethyl) disulfaneyl)ethyl (1-((2R,4R,5R)-3,3-difluoro-4-hydroxy-5-(hydroxymethyl)tetrahydrofuran-2-yl)-2-oxo-1,2-dihydropyrimidin-4-yl)carbamate (2)

A solution of GEM (263 mg; 1 mmol) and TEA (303 mg; 3 mmol) in 10 mL DMF was added slowly to a solution of compound **1** (1.44 mg, 3 mmol) in 5 mL DMF and then stirred for 12 h at room temperature. Upon completion of reaction, the solvent was removed and the solid was dissolved in 100 mL DCM. The solution was then washed with ultrapure water and the organic phrase was then collected and concentrated in vacuo. The crude product was purified by column chromatography on silica gel (DCM:MeOH, 20:1) to obtain compound **2** (295 mg, 48.1%) as a yellow solid. ^{1}H NMR (500 MHz, DMSO-d_6) δ 8.38−8.29 (m, 1H), 8.14−8.10 (m, 1H), 7.65 (d, J = 7.5 Hz, 1H), 7.61−7.53 (m, 1H), 7.45 (d, J = 9.4 Hz, 2H), 6.97−6.89 (m, 1H), 6.23 (d, J = 9.9 Hz, 1H), 5.81 (dd, J = 7.5, 1.3 Hz, 1H), 5.27 (t, J = 5.9 Hz, 2H), 4.58−4.27 (m, 4H), 4.25−4.14 (m, 1H), 3.74 (s, 1H), 3.71 (s, 1H), 3.69−3.62 (m, 1H), 3.07 (d, J = 53.7 Hz, 1H). MS (ESI): $[M+H]^+$: 609.8.

2.4. Synthesis of cationic polymer prodrug GEM-SS-PC

Compound **2** (608 mg, 2 mmol) and TEA (1.12 g, 10 mmol) were mixed in 5 mL DMF, and then added in 10 mL PC solution (3 g, dissolved in 10 mL DMSO) stirred at room temperature. After stirring for 12 h, DMF was removed and dialyzed against ultrapure water for 24 h. The dialyzate was freeze-dried to obtain the white power PC. The chemical structures were determined by ^{1}H NMR.

2.5. Preparation of Er@PC and the co-delivery system Er@GEM-SS-PC

The Er@PC and the co-delivery system Er@GEM-SS-PC were obtained by host–guest interaction. Briefly, Er (21.5 mg) was dissolved in acid solution (0.5 mol/L acetic acid), and the Er solution was added dropwise to the PC (100 mg in 0.5 mol/L acetic acid solution) or GEM-SS-PC solution (200 mg in 0.5 mol/L acetic acid solution). The above mixture was stirred until all substances completely dissolved, and then freeze-dried for 48 h to yield yellowish powders. The chemical structures were determined by ^{1}H NMR. For determination of Er loading in the Er@GEM-SS-PC, the freeze-dried Er@GEM-SS-PC (5 mg) was dissolved in 5 mL DMSO and the concentration of Er in the Er@GEM-SS-PC was determined based on its UV absorbance intensity at λ = 330 nm. The drug loading rate (DLR) was calculated as 26.3% according to the following Eq (1):

$$\text{DLR}\ (\%) = \text{Mass of loaded Er} / \text{Mass of Er@GEM-SS-PC} \times 100 \quad (1)$$

2.6. Electrophoretic gel assay

Free IRAK4 siRNA (siIRAK4), siIRAK4/Er@GEM-SS-PC, and siIRAK4/Er@GEM-SS-PC-M (in PBS or serum) were mixed with loading buffer and loaded into 2% agarose gel. Electrophoresis was conducted in 1 × Tris-acetate-EDTA (TAE) buffer at 120 V for 15 min in a JUNYI Electrophoresis Equipment (JY300, Beijing Junyi-Dongfang, Beijing, China). The resulting gels were analyzed using a UV illuminator (FluorChem E System, ProteinSimple, CA, USA). RNA bands were visualized and imaged by a Gel Documentation System (C150, Azure Biosystems, CA, USA).

2.7. Cell culture

The human pancreatic cancer cell line PANC-1 and SW1990 were purchased from the American Type Culture Collection (ATCC, VA, USA). SW1990-luci (luciferase-expressing SW1990) cells were purchased from the Sciencelight Biology Science & Technology Co., Ltd. (Shanghai, China). The cells were grown in Dulbecco's modified Eagle's medium (DMEM) containing 10% fetal bovine serum (FBS) in a humidified atmosphere of 5% CO_2 and 95% air at 37 °C. Mycoplasma testing using the MycoAlert Mycoplasma Detection Kit (LT07-318, Lonza, MD, USA) was performed every 3 months.

2.8. Western blot analysis

Cells were cleaved with RIPA lysate (R0010, Solarbio, Beijing, China). The hENT1 membrane protein was extracted according to the membrane protein extraction kit (P0033, biyuntian, Shanghai, China). The total protein was quantified by the BCA protein assay kit (23225, Promega, WI, USA) and equalized before loading. Equal amounts of protein extracts were subjected to electrophoresis in SDS-polyacrylamide gels and transferred to polyvinylidene fluoride (PVDF) membranes. The membranes were then blocked with 5% nonfat milk and cultured overnight at 4°C with the primary antibodies against hENT1 (1:1000), EGFR (1:1000), p-EGFR (1:1000), IRAK4 (1:1000), NF-κB (1:2000), NF-κB p65 (1:2000) and GAPDH (1:1000). The blots were washed, incubated with a peroxidase-conjugated antibody, and chemiluminescence detection was performed using an enhanced chemiluminescence kit according to the manufacture's protocol (32209, Thermo Scientific™, IL, USA). Band intensity was quantified by densitometric analysis using the NIH Image J Program (http://rsb.info.nih.gov/ij/). The relative expression was normalized to the expression of GAPDH.

2.9. In vitro cellular internalization of NPs

The cell internalization behaviors of ICG-labeled siIRAK4/Er@GEM-SS-PC-M were investigated by CLSM. Briefly, SW1990 and PANC-1 cancer cells were seeded into dishes at a density of 5 × 10^4 cells. After 24 h of incubation, siIRAK4/Er@GEM-SS-PC-M was added and incubated with or without

the 50 mmol/L dilazep (hENT1 inhibitor) at 37 °C for 12 h. Then, the medium was removed and washed three times with PBS. The cancer cells were fixed with 4% formaldehyde and subsequently stained with DAPI. Fluorescent images were captured by CLSM.

2.10. 3D tumor spheroid culture and penetration assay

The 3D tumor spheroid was constructed. Briefly, 40 μL of hot agarose solution (2%) was added quickly into the 96-well plate per well. After the agarose solution was solidified, the spheroid was seeded by suspending the PANC-1 cells and L929 fibroblasts at the ratio of 1:2, and adding at the density of 10^4/mL at the volume of 200 μL per well. Then, the spheroids were cultured at 37 °C with 5% CO_2 for 10 days to form the 3D tumor spheroid for the penetration study. The penetration capability of ICG and ICG labeled siNT/Er@GEM-SS-PC-M, siIRAK4/Er@GEM-SS-PC and siIRAK4/Er@GEM-SS-PC-M were evaluated by the fluorescence intensity at different scanning depth (from 0 to 75 μm) with confocal microscopy using Z-Stack mode (LSM 880 with fast AiryScan, Zeiss, Jena, Germany). Image analysis of the fluorescence was performed by using ImageJ.

2.11. Biodistribution study

In vivo imaging study of the nanoparticle distribution was performed on mice bearing subcutaneous tumors intravenously injected with free ICG or ICG labeled NPs. Anesthetized by isoflurane, the mice were photographed under IVIS spectrum imaging system at Ex/Em 788 nm/808 nm at 2, 4, 8, 12 and 24 h post injection. The tissues and main organs (heart, liver, spleen, lung, kidney and tumor) were collected and photographed at 24 h.

2.12. Immunofluorescence

The specimens were labeled with antibodies against NF-κB p65 (10745-1-AP) or α-SMA (Abcam, ab64693) overnight at 4 °C for co-localization detection. After washing, the sections were incubated with a mixture of Alexa Fluor 488- and Alexa Fluor 594-conjugated secondary antibodies for 1 h. Then, the specimens were washed with phosphate buffered saline (PBS), and then mounted with fluorescent mounting medium containing 4′,6-diamidino-2-phenylindole (DAPI). Each section was observed by using a confocal microscopy (Carl Zeiss, Germany).

2.13. Tumor model and treatment regimes

Athymic BALB/c mice (16−20 g, 4−6 weeks old) were housed on a 12-h light/12-h dark cycle in a pathogen-free environment, and allowed *ad libitum* access to food and water. The animal experiments were approved by the Sir Run Run Shaw Hospital Institutional Animal Care and Use Committee and conducted according to the Guide for the Care and Use of Laboratory Animals of Zhejiang University, Hangzhou, China.

To establish the orthotopic pancreatic cancer model, the luciferase-expressed SW1990 pancreatic cancer cells (2×10^6 in 25 μL of PBS) into the pancreatic tail of BALB/c nude mice. After injection of the cancer cells for about 7 days, the orthotopic pancreatic tumor-bearing mice were established, and randomly divided into five group, and administered intravenously with free GEM (2 mg/kg per mouse) combined with Er (2 mg/kg per mouse), siNT/Er@GEM-SS-PC-M (at the dose of 2 mg/kg Er and 2 mg/kg GEM), siIRAK4/Er@GEM-SS-PC (at the dose of 2 mg/kg Er and 2 mg/kg GEM) and siIRAK4/Er@GEM-SS-PC-M (at the dose of 2 mg/kg Er and 2 mg/kg GEM) or vehicle once weekly for two weeks. Animal care technicians were blinded to the treatment groups. Tumor growth was detected by an ex *vivo* luciferase-based noninvasive bioluminescence imaging system (IVISR Spectrum, PerkinElmer) after injection of 2 mg D-Luciferin potassium salt per mouse. One-half of the mice were sacrificed by cervical vertebra dislocation 21 days after tumor implantation, the tumor tissues, peripheral blood and the major organ of mice were collected. The remaining mice were used for the survival study and sacrificed when the mice became moribund. Survival rate was determined from the first day of implantation until Day 60.

For the patient-derived tumor xenograft, the patients were fully informed and signed a written informed patient consent form. The Ethics Committee of Sir Run Run Shaw Hospital, Zhejiang University School of Medicine, approved the experimental protocol. The human pancreatic cancer tissue specimens were collected under sterile conditions in antibiotic-containing PBS medium and immediately transplanted as 2−3 mm^3 pieces into subcutaneous pockets of athymic nude mice. Tumors from the first generation of mice were harvested when the tumor volume reached approximately 1.5 cm^3, following re-implanted into a new generation of nude mice as the second generations. The third generation of nude mice bearing tumors were used for the further experiments and randomly divided into five groups as indicated above. The mice were administered intravenously with the combination of free GEM (2 mg/kg per mouse) and Er (2 mg/kg per mouse), siNT/Er@GEM-SS-PC-M (at the dose of 2 mg/kg Er and 2 mg/kg GEM), siIRAK4/Er@GEM-SS-PC (at the dose of 2 mg/kg Er and 2 mg/kg GEM) and siIRAK4/Er@GEM-SS-PC-M (at the dose of 2 mg/kg Er and 2 mg/kg GEM) or vehicle once weekly for five weeks, starting on Day 7 after tumor implantation. Animal care technicians were blinded to the treatment groups. The tumor volume was measured and calculated by Eq. (2):

$$\text{Tumor volume} = 0.5 \times \text{Length} \times \text{Width}^2 \quad (2)$$

The mice were sacrificed by cervical vertebra dislocation on Day 45 after the tumor implantation, the tumor tissues, peripheral blood and the major organ of mice were collected for further analysis. For the survival study, the mice were sacrificed when the length of the tumor exceeded 2 cm or they became moribund. Survival rate was determined from the first day of implantation until Day 80.

2.14. Immunohistochemistry

For the immunohistochemistry staining of ki67 and α-SMA, the tumor tissue section was incubated with antibody against rat ki67 (1:200) or α-SMA (1:200) in a humidified chamber overnight at 4 °C. Then followed by incubation with HRP-conjugated secondary antibody at 37 °C for 1 h and reacted with 3,3′-diaminobenzidine tetrahydrochloride (DAB). Images were captured

with a phase-contrast microscope (cx41, Olympus Corporation, Tokyo, Japan). The numbers of positive cells were recorded. Every fifth section was used for stereological assessment.

2.15. Statistical analysis

All data were analyzed by Graphpad prism 8.0. Biological replicates were used in all experiments unless stated otherwise. Data were presented as mean ± standard deviation (SD). The Kaplan−Meier method and the log-rank test were used to evaluate the survival rates. Unpaired two-tailed Students' *t*-test was used for comparison of two groups. Two-way ANOVA with a Bonferroni *post-hoc* test was used when both time and treatment were compared. The *P*-value less than 0.05 was considered significant ($^{*}P < 0.05$, $^{**}P < 0.01$, $^{***}P < 0.001$, $^{****}P < 0.0001$).

3. Result and discussion

3.1. Synthesis and characterization of siIRAK4/Er@GEM-SS-PC-M

In our study, the β-CD was crosslinked with the low molecular weight PEI (∼600 Da) *via* CDI-activated condensation reaction to obtain the cationic polymer vector PC (Supporting Information Scheme S1) in accordance with our previous reports[37−39]. As shown in Supporting Information Fig. S1, ^{1}H NMR of PC shown that there was about 2.4 mmol of PEI conjugated to every 1 mmol of β-CD. For this vector, the hydrophobic cavity of β-CD segment displayed the ability to form the complex with the hydrophobic small molecule drug Er *via* host–guest interaction, which contributed to the improved drug stability and water solubility. Meanwhile, the PEI segment not only acted as the delivery carrier for siRNA with high transfection efficiency, but also exhibited low toxicity due to the low molecular weight. Notably, the carbamate linkage of β-CD and PEI had been gradually degraded under the physiological environment, indicating the good biocompatibility and low cytotoxicity. The GEM was succeeded in conjugating the polymeric backbone of PC by −SS− bond linker *via* 3-step reactions, which formed a GSH-responsive cationic polymer prodrug GEM-SS-PC (Supporting Information Scheme S2). The PC, GEM-SS-PC and its intermediates were characterized by ^{1}H NMR and MS (Supporting Information Figs. 1–5). For the co-delivery of Er and GEM in this polymer prodrug, the Er in acid solution (0.5% acetic acid) was gradually added to the GEM-SS-PC solution (0.5% acetic acid) to form the co-delivery system Er@GEM-SS-PC (Fig. 1A). As shown in Fig. 1B, we could observe a new multiplet corresponding to the aromatic proton of Er appeared at σ 7.0−8.5 ppm in ^{1}H NMR, which proved that the GEM-SS-PC could load the Er to form the co-delivery system Er@GEM-SS-PC. Moreover, the two-dimensional nuclear overhauser effect spectroscopy (2D-NOESY) further revealed that the aromatic segment of Er was well correlated with the PC segment of GEM-SS-PC, indicating that the Er generated supramolecular inclusion complex with GEM-SS-PC *via* the host–guest interaction (Supporting Information Fig. S6). We also investigated the ratio of Er to GEM in Er@GEM-SS-PC. Based on ^{1}H NMR, the peak area of typical protons on H1 (Er) and H2 (GEM) were comparable, suggesting that the molar ratio of Er to GEM was close to 1:1 (Supporting Information Fig. S7 and Table 1). Moreover, the peak area ratio of typical protons on H3 (PC) to H1(Er) was 6.3:1, indicating that the molar ratio of loaded Er to GEM-SS-PC was 1.1:1. We also estimated that the molar ratio of GEM in Er@GEM-SS-PC was 1:5.7, which calculated that 1.25 GEM molecules were conjugated to one molecule of PC. In addition, the absorption spectra for Er@GEM-SS-PC shown in Fig. 1C displayed two absorption bands, one appeared at 330 nm and the other at 270 nm, which was consistent with the absorption band of Er (330 nm) and GEM (270 nm), further demonstrated that the Er was loaded into the cavity of GEM-SS-PC. Due to the positively charged cationic character of PEI segment in Er@GEM-SS-PC, this cationic co-delivery system was able to complex with siRNA and condensed into NPs for achieving the co-delivery of gene therapeutic agents. By mixing the Er@GEM-SS-PC with siIRAK4, as shown in Fig. 1D, the resulted complexes (siIRAK4/Er@GEM-SS-PC) were determined by dynamic light scattering (DLS) and found that the average particle size was about ∼150 nm, and the morphology observed on a transmission electronic microscope (TEM) displayed compact spherical NPs. To further examine the ability of Er@GEM-SS-PC to complex the siRNA, the agarose gel electrophoresis assay was performed in Fig. 1E, and found that the migration of siIRAK4 was totally inhibited by Er@GEM-SS-PC when the *N*/*P* ratio reached 8:1 (Fig. 1E). Given that the stimuli-responsive drug release in nano-drug system can reduce side effect and enhance accumulation of the active drug in tumor cells, the drug release behavior of siRNA/Er@GEM-SS-PC was evaluated under the GSH or acid rich environment. As shown in Fig. 1F, after incubation with 10 mmol/L GSH in pH 7.4 PBS, the siIRAK4/Er@GEM-SS-PC progressively released GEM due to the cleavage of the −SS− bond, and the cumulative percentage of release was over 50% at 8 h and reached its maximum at around 12 h, while it is negligible drug release under physiological environment and low drug release in low concentration of GSH, implying the GSH in high concentration can trigger the −SS− linker and release anticancer drug GEM. We also measured the response of siRNA/Er@GEM-SS-PC to GSH by TEM image, as shown in Supporting Information Fig. S8, which indicated that the NPs of siRNA/Er@GEM-SS-PC were aggregated and deformed after incubation with 10 mmol/L GSH at the same condition. Moreover, the release profiles of siRNA were performed by the agarose gel electrophoresis assay, as shown in Fig. 1E, the migration was recovered in the GSH rich environment, suggesting that GSH broke the stability of the nanocomplex and promoted the release of siIRAK4. In our previous similar study[33], the increased water solubility of the hydrophobic drug within β-CD can trigger the disassembly of the host–guest interaction on hydrophobic drug and β-CD, which induces the hydrophobic drug release from the cavity of β-CD. However, the Er is difficult to dissolve in physiological environment (pH 7.4), while the water solubility of Er enhanced quickly when the pH dropped[40,41]. As shown in Fig. 1G, the siRNA/Er@GEM-SS-PC were stable at pH 7.4, and less than 20% of Er was released within 24 h. By contrast, at pH 5.0, the intracellular endo/lysosomal environment, we observed rapidly Er release within the first 4 h and reached a plateau at 80% within 12 h due to the enhanced water solubility of Er. Recently, many works proved that the elevated GSH level in the tumoral and intracellular environment can cleave the disulfide bonds to disassemble the nanoparticle and release the drug[42−44]. The cleavage of the disulfide bond can trigger a cascade of self-eliminations reactions[45,46], which is likely to cleave the amide ester linking β-

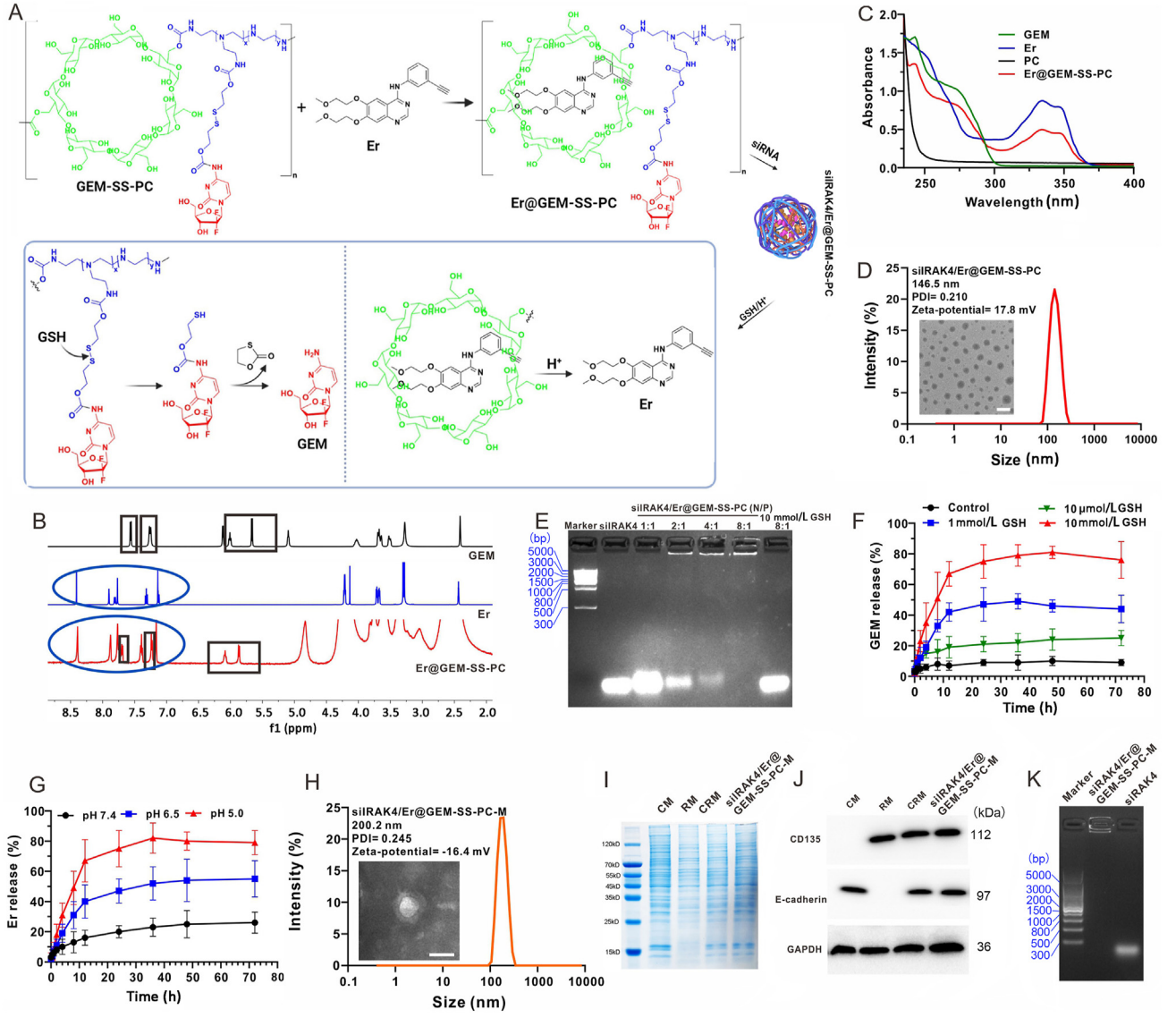

Figure 1 Synthesis and characterization of membrane-coated drug-delivery nano-drug siIRAK4/Er@GEM-SS-PC-M. (A) The preparation of the co-delivery system Er@GEM-SS-PC and nano-drug siIRAK4A/Er@GEM-SS-PC and the GSH/pH responsive release process of siIRAK4/Er@GEM-SSPC (Er: triggered by the acid; GEM: triggered by the GSH); (B) The ^{1}H NMR of Er@GEM-SS-PC, Er and GEM; (C) Absorption spectra for Er@GEM-SS-PC, Er, PC and GEM in pH 7.4 PBS solution (containing 50% DMSO); (D) The diameter distribution as determined by DLS and the TEM image for siIRAK4/Er@GEM-SS-PC. Scale bar = 200 nm. (E) Agarose gel electrophoresis assay of Er@GEM-SS-PC with siIRAK4 at different *N*/*P* ratios. (F) The cumulative release profiles (by HPLC) for GEM siIRAK4A/Er@GEM-SS-PC, which triggered by different GSH concentration (0−10 mmol/L); (G) The cumulative release profiles (by HPLC) for Er from siIRAK4/Er@GEM-SS-PC by different pH values (5.0, 6.5 and 7.4); (H) The diameter distribution as determined by DLS and the TEM image for hybrid membrane-coated nanoparticles siRNA/Er@M-GEM-SS-PC. Scale bar = 200 nm. (I) SDS-PAGE analysis of SW1990 cancer cell membrane (CM), RAW264.7 macrophage membrane (RM), hybrid membranes (CRM) and siIRAK4/Er@GEM-SS-PC-M (hybrid membrane-coated). (J) Western blot analysis of cell membrane specific proteins of SW1990 (E-cadherin), RAW264.7(CD135), hybrid membranes and siIRAK4/Er@GEM-SS-PC-M. (K) Agarose gel electrophoresis assay of siIRAK4/Er@GEM-SS-PC-M.

CD and low-molecular-weight PEI and trigger the release of siRNA, as shown in Supporting Information Fig. S9A. In order to verify the release behavior of siRNA, high resolution electrospray ionization mass spectrometry (ESI-HRMS) was performed after incubating with siIRAK4@GEM-SS-PC or siIRAK4/Er@GEM-SS-PC with GSH (10 mmol/L GSH, 12 h). In Fig. S9B, the anticipated disassembly of siIRAK4/GEM-SS-PC was observed at ESI-HRMS analysis. We found there was one ionic peak corresponding to β-CD ($[M+H]^+$ = 1135.3760) in ESI-HRMS as well as the other for GEM ($[M+H]^+$ = 264.0791), suggesting the cleavage of both disulfide and methyl carbamate bonds. All these results confirmed that the high level of GSH can disassemble the polymeric carrier, and release the GEM and siRNA. These results demonstrate that Er@GEM-SS-PC can load siRNA to form nano-complexes (siIRAK4/Er@GEM-SS-PC) and the GSH-overexpression/acid environment can induce the sustained release of the parent drugs GEM and Er.

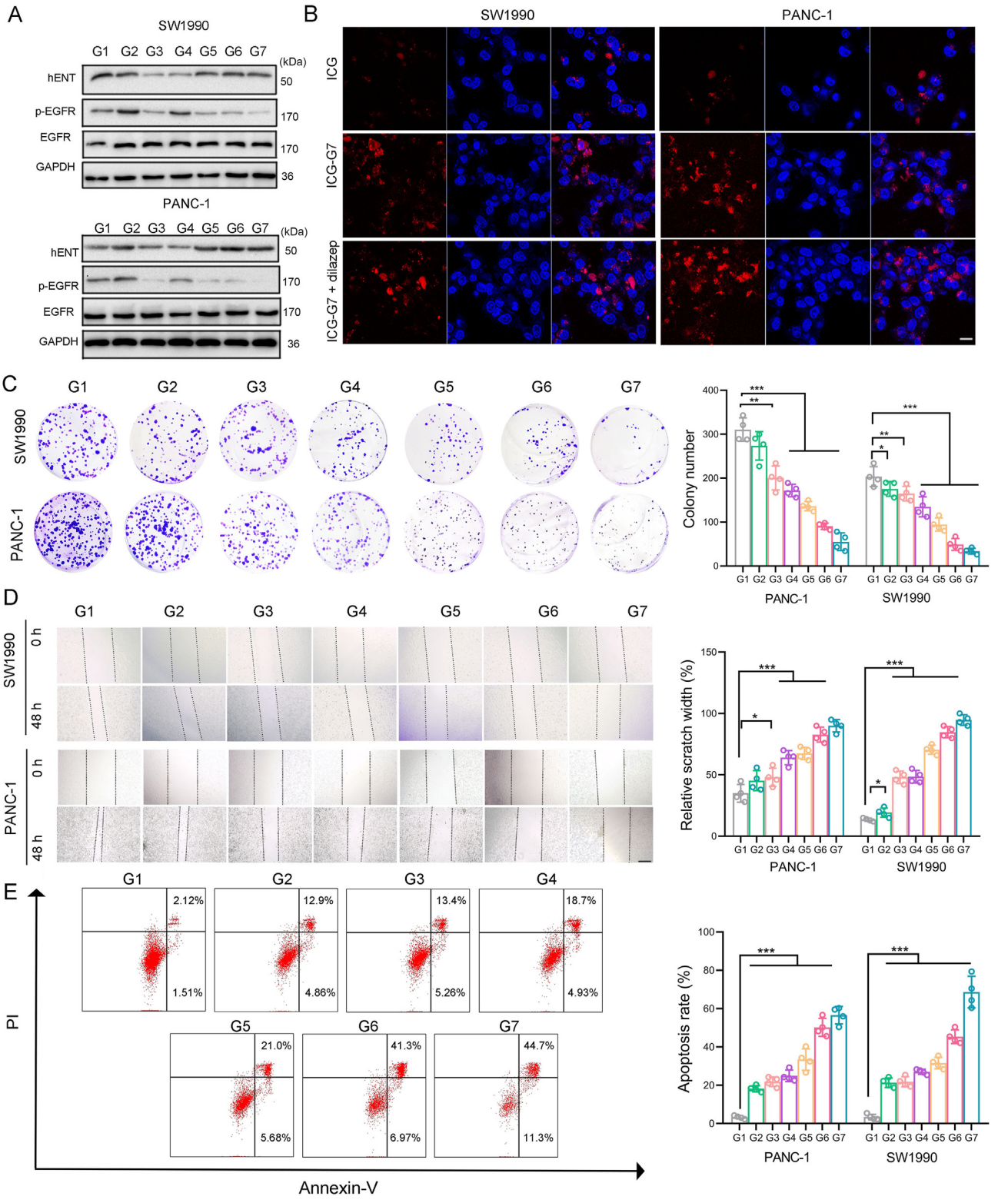

Figure 2 siIRAK4/Er@GEM-SS-PC-M blocks the antagonism between the GEM and Er and facilitates the *in vitro* antitumor activity. (A) The SW1990 and PANC-1 cells were incubated with GEM, Er, free GEM and Er, siNT/Er@GEM-SS-PC, siIRAK4/Er@GEM-SS-PC and siIRAK4/Er@GEM-SS-PC-M for 24 h. The protein expression of hENT1, p-EGFR and EGFR was determined by Western blot. G1, PBS; G2, GEM; G3, Er; G4, free GEM and Er; G5, siNT/Er@GEM-SS-PC; G6, siIRAK4/Er@GEM-SS-PC; G7, siIRAK4/Er@GEM-SS-PC-M. (B) The SW1990 and PANC-1 cells were pre-incubated with or without dilazep (a hENT1 inhibitor) and then treated with the free ICG or ICG-labeled siIRAK4/Er@GEM-SS-PC-M for 24 h. Confocal images of the above treated cells. Scale bar = 10 μm. (C) Colony-formation assays were conducted to determine the proliferation of the SW1990 and PANC-1 cells receiving the above indicated treatment. (D) Scratch wound assay was performed to determine the migration capability of the above treated cells. The images in each group were obtained by microscopy at 0 and 48 h after the cells were scratched. Scale bar = 200 μm. (E) Apoptosis in SW1990 cells was determined by Annexin-V and PI staining and detected by flow cytometry analysis (mean ± SD, $n = 4$).

Many reported works have proved that cationic polymer can selectively concentrate drug molecules at the tumor site by permeability and retention (EPR) effect and functional modification[47−51]. To decrease the MPS-mediated clearance during systemic circulation and enhance the tumor targeting capability, the related cancer cell-macrophage hybrid membrane reported previously[36] was coated on the siIRAK4/Er@GEM-SS-PC NPs to form biomimetic nano-drug siIRAK4/Er@GEM-SS-PC-M. The DLS showed that the size of biomimetic NPs was larger compared to the siIRAK4/Er@GEM-SS-PC NPs (200 nm *vs.* 146 nm), and the surface zeta potential decreased from 17.8 to −16.4 mV after hybrid membrane coating (Fig. 1H), thus confirming the presence of the negatively charged outer membrane layer. To confirm whether the membrane proteins were still reserved after coating on the NPs, the total proteins of the hybrid membranes were examined by sodium dodecyl sulphate-polyacrylamide gel electrophoresis (SDS-PAGE). As shown in Fig. 1I, the protein profiles from siIRAK4/Er@GEM-SS-PC-M were almost identical to that of the native hybrid membranes. Furthermore, the specific membrane proteins of both cell types were detected in the hybrid membranes and siIRAK4/Er@GEM-SS-PC-M (Fig. 1J and Supporting Information Figs. S10 and S11). Noted that CD45 and CD14 were still reserved in the CRM-coated NPs, which might help the nanoparticle evade from MPS-mediated clearance. In Fig. 1K, we also observed that the hybrid membrane coating did not affect the capability of Er@GEM-SS-PC to complex siRNA. The stability of the NPs was analyzed in serum, it was noted that the siIRAK4/Er@GEM-SS-PC NPs were observable for 24 h in serum, whereas most of free siIRAK4 was degraded (Fig. S11). Importantly, the siIRAK4/Er@GEM-SS-PC-M were more stable at 24 h in the serum as compared with the naked siRNA and siIRAK4/Er@GEM-SS-PC (Supporting Information Fig. S12). As shown in Supporting Information Fig. S13, siIRAK4/Er@GEM-SS-PC-M under GSH concentration (10 mmol/L) can release about 60% GEM at 36 h, which was less than that released by siIRAK4/Er@GEM-SS-PC. The similar result was observed for pH-triggered release of Er in siIRAK4/Er@GEM-SS-PC-M. Together, these results indicate that the membrane-coated siIRAK4/Er@GEM-SS-PC-M NPs are successfully synthesized and maintain the co-delivery function.

3.2. *siIRAK4/Er@GEM-SS-PC-M blocks the antagonism between the GEM and Er in vitro*

Previous study suggests that the limited combination efficacy of GEM and Er attribute to the inhibition effects of Er on the transportation protein hENT1, which is crucial for GEM accumulating in tumor cells[14]. We herein investigated whether Er treatment inhibits the hENT1 expression in SW1990 and PANC-1 pancreatic cancer cells, and found that free Er alone or in combination with GEM could reduce the expression of hENT1 as compared with the control (Fig. 2A), which was similar with the previous report[14]. Meanwhile, the phosphorylation level of EGFR and the expression of ERBB2 were augmented by free GEM treatment, and the EGFR and ERBB2 inhibition effects of Er were attenuated when combined with GEM (Fig. 2A and Supporting Information Fig. S14). It was evident that siIRAK4/Er@PC and siNT/Er@PC (siNT refers to scrambled siRNA) could significantly decrease the p-EGFR and ERBB2 without inhibiting the expression of hENT1. By contrast, siIRAK4/GEM-SS-PC and siNT/GEM-SS-PC enhanced the expression of p-EGFR and ERBB2 (Fig. S14). Notably, siNT/Er@GEM-SS-PC-M, siIRAK4/Er@GEM-SS-PC, or siIRAK4/Er@GEM-SS-PC-M treatment displayed almost no inhibition effect on hENT1 expression, and the phosphorylation level of EGFR and the expression of ERBB2 were drastically attenuated by the above treatments (Fig. 2A, Supporting Information Fig. S15), suggesting the unfavorable antagonism between the free GEM and Er was abolished *via* the nano-carrier mediated drug co-delivery system. To elucidate the potential mechanism of decreased antagonism, we first used dilazep (an hENT1 inhibitor for GEM intracellular uptake) to pretreat the pancreatic cancer cells, which were then incubated with the ICG-labeled siIRAK4/Er@PC, siIRAK4/GEM-SS-PC, siNT/Er@PC, siNT/GEM-SS-PC and siIRAK4/Er@GEM-SS-PC-M (Fig. 2B and Supporting Information Fig. S16). We found that the above NPs were independent of hENT1 in terms of cellular uptake by pancreatic cancer cells, which indicated that GEM-loaded NPs have changed the mode of cellular uptake, as opposed to free GEM and may also contribute to the decreased antagonism with Er.

3.3. *In vitro synergistic anti-proliferation, anti-migration and pro-apoptosis effects of siIRAK4/Er@GEM-SS-PC-M*

Next, the anti-proliferation activity of different treatment groups was evaluated by pre-incubating pancreatic cells with free or conjugated drugs and determined by colony formation experiments. As shown in Fig. 2C, the number of colonies was significantly diminished by the combination of free GEM and Er treatment as compared with the control. Interestingly, although the antagonism between GEM and Er was observed, the combination of the GEM and Er has been validated to display superior anti-proliferation effects to gemcitabine alone in PANC-1 cells, as previously observed in various cell types of cancers including pancreatic cancer[11,14,16]. Notably, siIRAK4/Er@GEM-SS-PC-M treatment drastically decreased the colony number of SW1990 and PANC-1 cells as compared with other treatment groups. Given that the pancreatic cancer is highly invasive tumor[52], we investigate whether siIRAK4/Er@GEM-SS-PC-M suppresses the migration of pancreatic cancer cells. As shown in Fig. 2D, the scratch distance in the GEM and Erl monotherapy was 1.43- and 3.56-fold higher than that in the control group for SW1990 cells, respectively, whereas the scratch distance in the free drug combination group was only 3.60-fold higher than that in the control. Importantly, the migration distance was drastically decreased in the siIRAK4/Er@GEM-SS-PC-M treatment group as compared with the other groups. Meanwhile, the pro-apoptosis effects of the co-delivery system were evaluated (Fig. 2E), and we found that the apoptosis rate of GEM, Er or their combination (GEM and Er) was 6.23-, 6.38- and 7.91-fold higher than that in the control group. Notably, the siIRAK4/Er@GEM-SS-PC-M treated SW1990 cells exhibited an almost 60% apoptosis rate, which was much higher than that of the other group. To further validate the synergistic effects of our nanodrugs, the coefficient of drug interaction (CDI) analysis was performed to determine drug interactions (*i.e.*, additive, synergistic, or antagonistic). We found that the CDI was 1.06 and 1.15 in the free GEM/Er combination group in terms of the anti-migration and pro-apoptotic effects for PANC-1, respectively, indicating the antagonistic interaction between the free drugs. By contrast, the designed nanosystem siIRAK4/Er@GEM-SS-PC-M revealed an excellent synergistic effect, with the CDI value of 0.11 and 0.49, respectively. The above results supported our hypothesis that the co-delivery nanosystem led to the synergistic effects. Similar results were

found in the SW1990 cells. Together, these results suggest that the siIRAK4/Er@GEM-SS-PC-M nanomedicine exerts superior synergistic anti-proliferation, anti-migration and pro-apoptosis effects *in vitro*.

3.4. *siIRAK4/Er@GEM-SS-PC-M promotes deep tissue penetrate in tumors*

Given that fibrotic pancreatic tumor microenvironment acted as a mechanical barrier to drug delivery, we explored whether our co-delivery system could impair the barrier and promote the deep tissue penetration of the nanomedicine. Among various pro-fibrotic pathways, the IRAK4/IL-1β pathway has been extensively studied due to its great value as a therapeutic target in pancreatic malignancy[31,32]. To this end, the specific siRNA against IRAK4 was designed and further optimized to achieve efficient knockdown of IRAK4 (Supporting Information Fig. S17). As shown in Fig. 3A, the hybrid membrane coated siIRAK4/Er@GEM-SS-PC displayed optative IRAK4 knock-down efficiency among groups. Inhibition of IRAK4 suppresses NF-κB-mediated production of pro-fibrotic cytokines IL-1β[31]. We demonstrate that blockade of IRAK4 by siIRAK4/Er@GEM-SS-PC-M attenuated NF-κB activation as evidenced by the decreased the nuclear translocation of p65 (Fig. 3B and C). Furthermore, the secretion of IL-1β were measured by the enzyme linked immunosorbent assay (ElISA), and we found that siIRAK4/Er@GEM-SS-PC-M drastically reduced the IL-1β secretion (Fig. 3D) as compared with the other groups. Next, we investigated the deep tissue penetration ability of the siIRAK4/Er@GEM-SS-PC-M NPs by 3D tumor spheroids. The NPs used

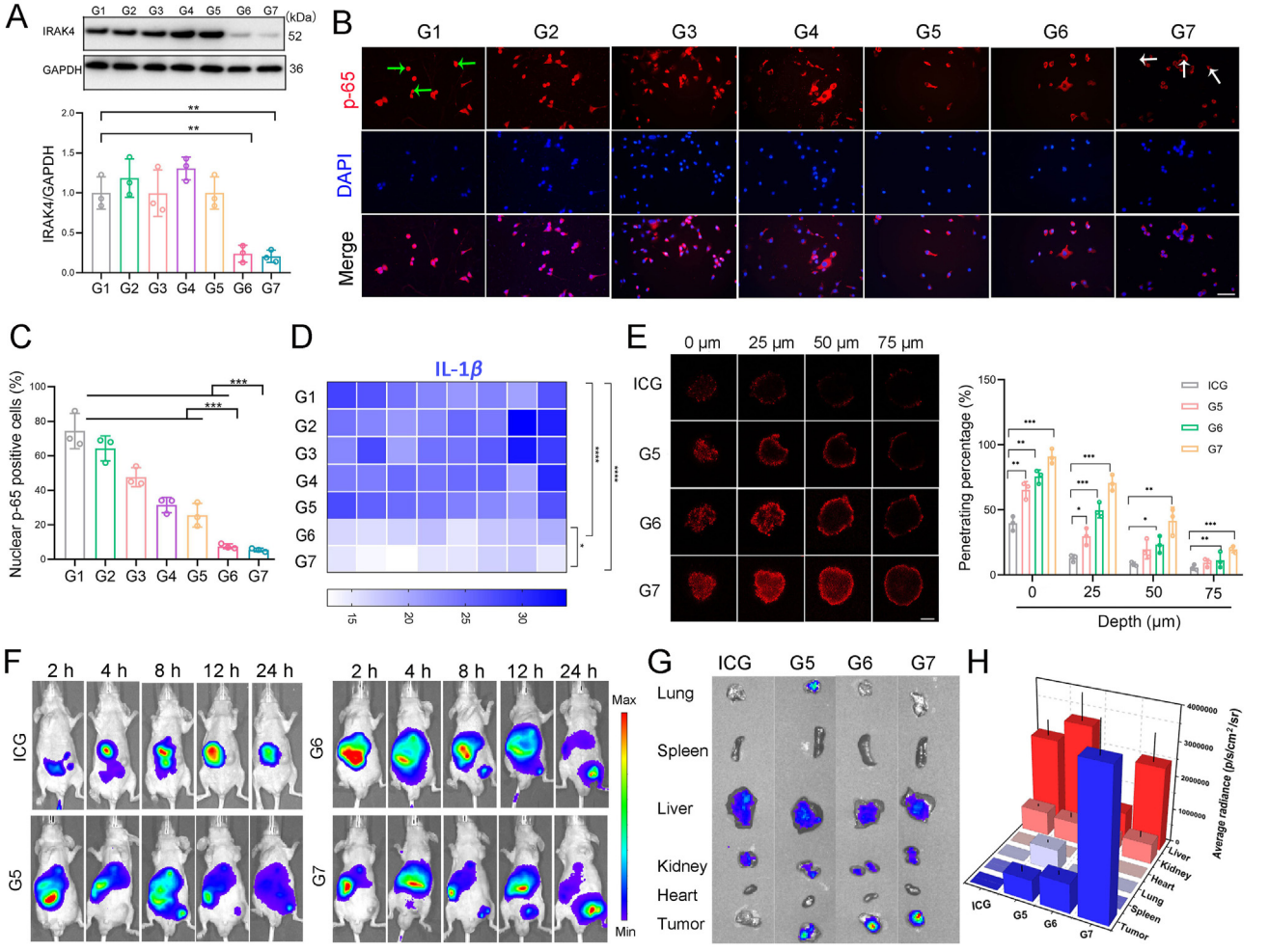

Figure 3 Blockade of IRAK4 pathway by siIRAK4/Er@GEM-SS-PC-M facilitates deep tissue penetrate in tumors. (A) The PANC-1 cells were treated with Gem, Er, free GEM and Er, siNT/Er@GEM-SS-PC, siIRAK4/Er@GEM-SS-PC and siIRAK4/Er@GEM-SS-PC-M for 24 h. The protein expression of IRAK4 was determined by Western blot. G1, PBS; G2, Gem; G3, Er; G4, free Gem and Er; G5, siNT/Er@GEM-SS-PC; G6, siIRAK4/Er@GEM-SS-PC; G7, siIRAK4/Er@GEM-SS-PC-M. (B, C) The localization of p-65 was examined by immunofluorescence staining. Scale bar = 50 μm. The green arrow indicated nucleus p-65, the white arrow indicated cytoplasm p-65 (mean ± SD, n = 3). (D) The secretion of IL-1β was determined by ELISA. (E) Fluorescence images and quantitative analysis of the penetration of free ICG and ICG-labeled NPs into 3D-cultured tumor spheroids. Images were acquired by CLSM at 0, 25, 50 and 75 μm distance from the top to the middle of the spheroid. Scale bar = 100 μm (mean ± SD, n = 3). (F) *In vivo* fluorescence imaging of the tumor bearing mice intravenously injected with free ICG, siNT/Er@GEM-SS-PC, siIRAK4/Er@GEM-SS-PC and siIRAK4/Er@GEM-SS-PC-M. All delivery vectors were labeled with ICG for fluorescence imaging. (G, H) Quantitative analysis of *in vivo* fluorescence intensity of dislodged organs harvested 24 h after the injection of NPs (mean ± SD, n = 3).

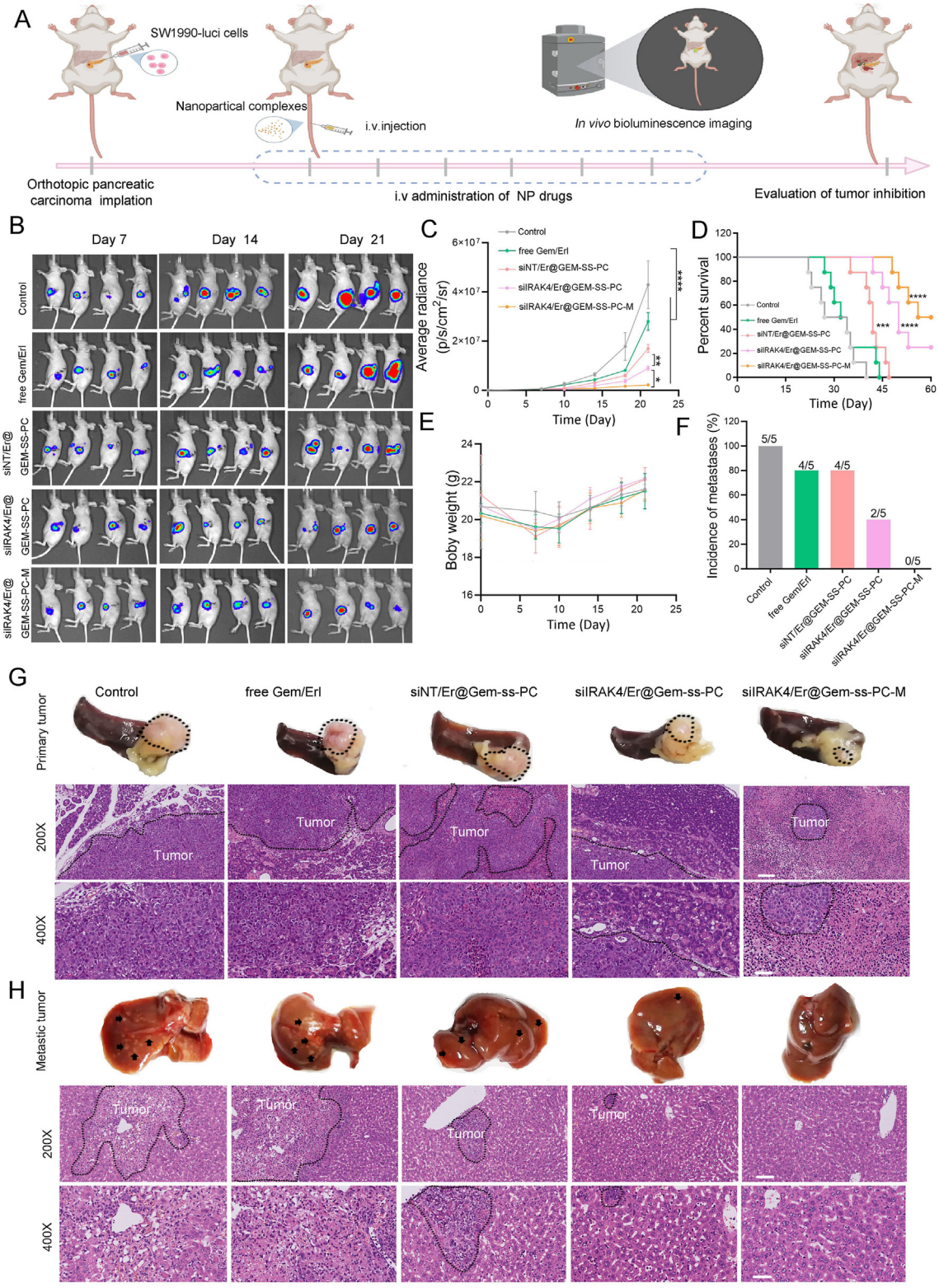

Figure 4 The anti-orthotopic tumor activity of the nano-drug siIRAK4/Er@GEM-SS-PC-M system. (A) The orthotopic pancreatic tumor-bearing mouse model was established after orthotopically injecting SW1990-luci cells in pancreatic tail for about 7 days. Then the mice were randomly divided into five groups and administrated twice a week with PBS, free GEM and Er, siNT/Er@GEM-SS-PC, siNT/Er@GEM-SS-PC, siIRAK4/Er@GEM-SS-PC and siIRAK4/Er@GEM-SS-PC-M for three weeks. (B) Representative *in vivo* bioluminescence images of mice receiving the above indicated treatment. (C) Quantitative analysis of bioluminescence intensity of mice bearing orthotopic pancreatic tumor (mean ± SD, $n = 5$). (D) The survival rate of the above treated mice was determined ($n = 8$, log-rank test). (E) The body weight of mice was

in this experiment were labeled with ICG and confirmed by the DLS and the TEM image (Supporting Information Fig. S18). The SW1990 cells were mixed with fibroblasts at the ratio of 1:2 to construct 3D tumor spheroids and mimic the morphology and microenvironment of pancreatic solid tumors. The fluorescence signal of ICG-labeled siNT/Er@GEM-SS-PC was primarily distributed on the periphery of the tumor spheroids, indicating the poor capability of siNT/Er@GEM-SS-PC to penetrate into deep tumor tissues. By contrast, both siIRAK4/Er@GEM-SS-PC and siIRAK4/Er@GEM-SS-PC-M could effectively penetrate deeper into the interior of the tumor spheroids at the distance of 50 μm (Fig. 3E). The *in vivo* fluorescence images of those NPs were further evaluated on the subcutaneous SW1990 tumor model by using the ICG fluorescence. As shown in Fig. 3F, the *in vivo* fluorescence in tumor tissue could be observed after intravenous injection of free ICG and ICG-labeled NPs. It was noted that mice injected with siIRAK4/Er@GEM-SS-PC-M displayed the strongest fluorescent intensity at the tumor site among the groups at 24 h post injection. The mice were subsequently sacrificed at 24 h post-injection, and fluorescence images of the *ex vivo* organs are displayed in Fig. 3H. Compared with the other groups, statistically more intense fluorescence signal from siIRAK4/Er@GEM-SS-PC-M group was distributed in tumor tissue after intravenous administration (Fig. 3G), indicating the tumor targeting ability by virtue of the immune escape and homotypic targeting of cancer cell−macrophage hybrid membrane. Together, these results suggest that siIRAK4/Er@GEM-SS-PC-M promotes deep tissue penetration in pancreatic tumors, which greatly encourages us to explore whether it could be extended to the potential therapeutic applications for cancer treatment.

3.5. *In vivo efficacy in orthotopic pancreatic tumor mode*

We subsequently evaluated whether such a co-delivery system could be translated into improved therapeutic efficacy in BALB/c nude mice bearing SW1990 orthotopic pancreatic tumors. The orthotopic pancreatic tumor-bearing mouse model was established after orthotopically injecting SW1990-luci cells in pancreatic tail for about 7 days. Then the mice were randomly divided into five groups and administrated twice a week with PBS, free GEM and Er combination, siNT/Er@GEM-SS-PC, siIRAK4/Er@GEM-SS-PC and siIRAK4/Er@GEM-SS-PC-M for three weeks (Fig. 4A). The distribution, size, and activity of orthotopic pancreatic tumors were noninvasively detected by bioluminescence emission after administration of 2 mg D-luciferin per mouse. The qualitative and quantitative time-dependent bioluminescent results of orthotopic pancreatic tumor-bearing mice in all groups were shown in Fig. 4B. It was noted that the combination of GEM or Er exhibited tumor growth inhibition, though statistical analysis did not reach significant (Fig. 4C). The siNT/Er@GEM-SS-PC treatment led to a significant restraint of tumor growth as compared with control (Fig. 4C). Importantly, the silRAK4/Er@GEM-SS-PC-M produced a more pronounced antitumor growth effect than other groups (Fig. 4C). The survival time of mice in the siIRAK4/Er@GEM-SS-PC-M was also greatly prolonged as compared with that in other groups (Fig. 4D). No significant loss of body weight was observed in the mice bearing-SW1990 tumors receiving the above indicated treatments (Fig. 4E). Given that pancreatic tumors prone to metastasis to the distant liver tissues, we subsequently detected the liver metastatic nodules of the mice receiving the indicated treatments, and found that the siIRAK4/Er@GEM-SS-PC-M greatly attenuated the liver metastasis of SW1990 tumor cells, while the hepatic metastatic symptom was obvious in other groups (Fig. 4F). The anti-tumor effects were also confirmed by the photograph of *ex vivo* excised orthotopic tumors, livers and the HE staining as intuitive evidence (Fig. 4G and H). Furthermore, HE staining revealed the good biocompatibility and safety by this therapeutic modality in the major organs (Supporting Information Fig. S19). These results suggest that the siIRAK4/Er@GEM-SS-PC-M we have developed is effective for the treatment of SW1990 orthotopic pancreatic tumors.

To further elucidate the mechanisms underlying the superior antitumor efficacy, we first estimated the expression of hENT and EGFR in tumor tissue by Western Blot assay. As shown in Fig. 5A and Supporting Information Fig. S20, the hENT1 expression was decreased by the combination of free GEM and Er, whereas the siNT/Er@GEM-SS-PC, siIRAK4/Er@GEM-SS-PC, siIRAK4/Er@GEM-SS-PC-M did not inhibit hENT1 expression with the attenuated phosphorylation of EGFR, suggesting that the antagonisms between the free GEM and Er were successfully abolished by the nano-carried mediated co-delivery systems. We then detected the expression IRAK4 and its downstream signal NF-κB, which contributes to the fibrosis process of tumor microenvironment. It was noted that the expression of IRAK4 and the phosphorylation of p65 was drastically downregulated after the siIRAK4/Er@GEM-SS-PC-M treatment (Fig. 5B, Fig. S20), accompanied by the reduced profibrotic cytokines IL-1β in the serum (Fig. 5C). Moreover, analyses of SW1990 tumor sections showed a significantly reduced degree of fibrosis evidenced by the Sirius Red$^+$ area and the α-SMA$^+$ fibroblasts (Fig. 5D and E), indicating the superior antifibrotic capability of our nano-drug. Finally, the Ki67 assay, and terminal deoxynucleotidyl transferase dUTP nick end labeling (TUNNEL) assay were conducted to assess proliferation and apoptosis levels in the tumor microenvironment. As shown in Fig. 5F−H, lowest proliferation (discerned by Ki67$^+$ staining) and highest apoptosis (by TUNNEL$^+$ staining) levels in tumor tissues were found in mice receiving siIRAK4/Er@GEM-SS-PC-M treatment. These results together indicate the successful reprogramming of tumor fibrosis microenvironment jointly by attenuated drug antagonisms in boosting the antitumor efficacy.

3.6. *In vivo efficacy in pancreatic PDX mode*

Encouraged by the excellent tumor growth inhibition ability on an orthotopic pancreatic tumor model, the *in vivo* antitumor activity of siIRAK4/Er@GEM-SS-PC-M was further evaluated on a PDX mode establish by pancreatic cancer patient derived specimens. Tissue specimens were transplanted as 2−3 mm^3 pieces into subcutaneous pockets of BALB/c nude mice as the first generation. The third generation of nude mice bearing tumors was used for further experiments and randomly divided into five groups (Fig. 6A). As shown in Fig. 6B and C, siNT/Er@GEM-SS-PC

measured (mean ± SD, $n = 5$). (F) Incidence of metastases in animals from the above treated groups. (G) Photograph of excised tumors with spleens in different treatment groups on Day 21. H&E staining of pancreatic tissues. Scale bar = 50 μm. (H) Photograph of excised liver in different treatment groups on Day 21. H&E staining of liver metastasis. Scale bar = 20 μm.

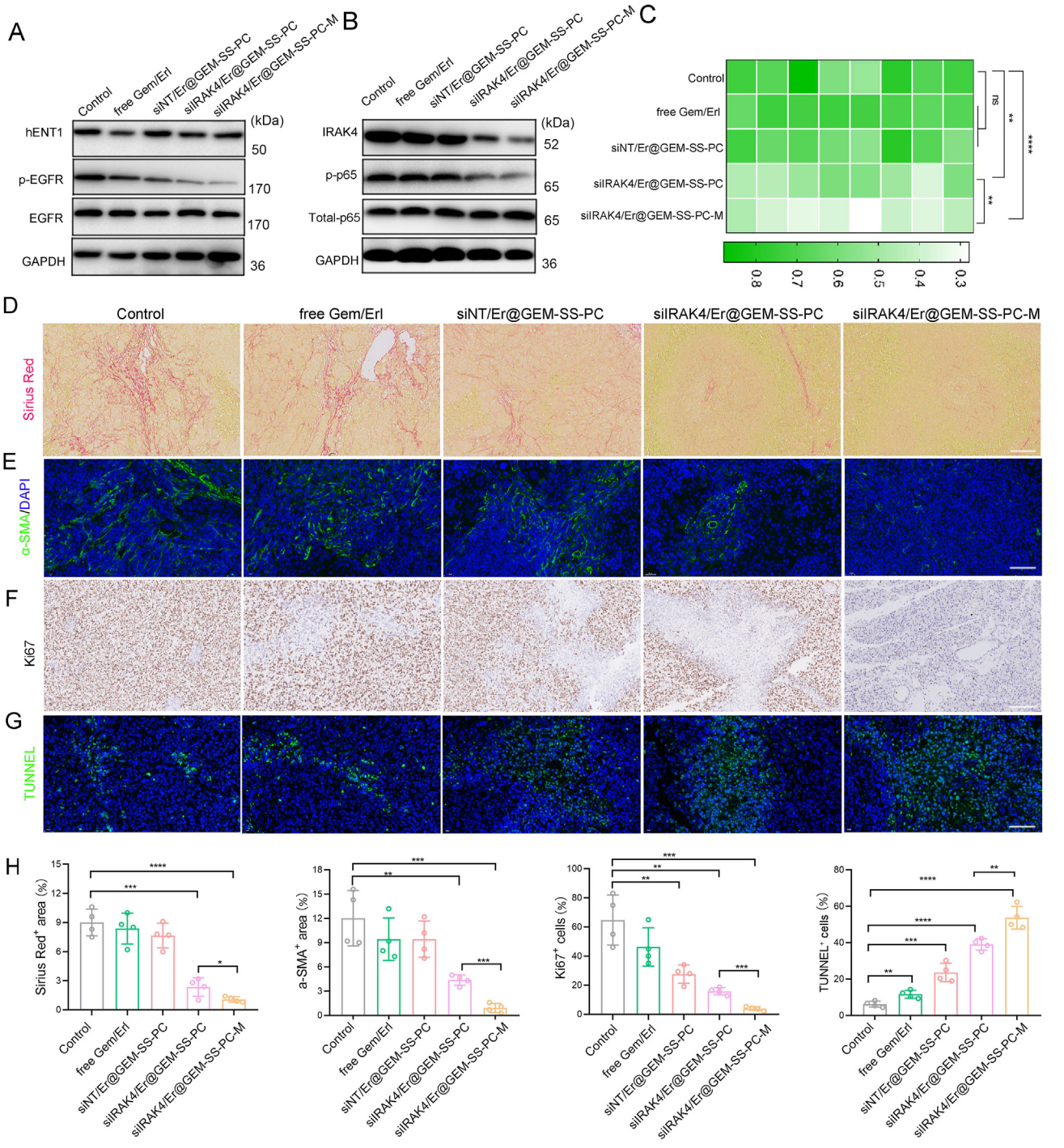

Figure 5 The nano-drug siIRAK4/Er@GEM-SS-PC-M reprograms fibrotic tumor environment. (A) The expression of hENT1 and the phosphorylation of EGFR were determined by Western blot. (B) The expression of IRKA4 and the phosphorylation of p-65 were determined by Western blot. (C) The secretion of IL-1β was determined by ELISA. (D) Representative images of Sirius Red positive area in tumors. Scale bar = 50 μm. (E) Representative images of α-SMA positive area in tumors. Scale bar = 50 μm. (F) Representative images of Ki67 positive area in tumors. Scale bar = 50 μm. (G) Representative images of TUNNEL positive area in tumors. Scale bar = 50 μm. (H) Quantitative analysis of Sirius Red, α-SMA, Ki67, TUNNEL positive area in tumors (mean ± SD, n = 4).

significantly inhibited tumor growth, whereas the combination of free GEM and Er did not restraint the tumor growth. The mice treated with siIRAK4/Er@GEM-SS-PC were more potent in delaying tumor growth compared with the siNT/Er@GEM-SS-PC treatment group, implying the complementary of anti-fibrosis therapy could efficiently initiate the synergistic anti-tumor effect. Importantly, after coating the cancer cell−macrophage hybrid membranes on the siIRAK4/Er@GEM-SS-PC, their anti-tumor growth effects were superior to all other groups due to the decreased MPS-mediated clearance and increased tumor

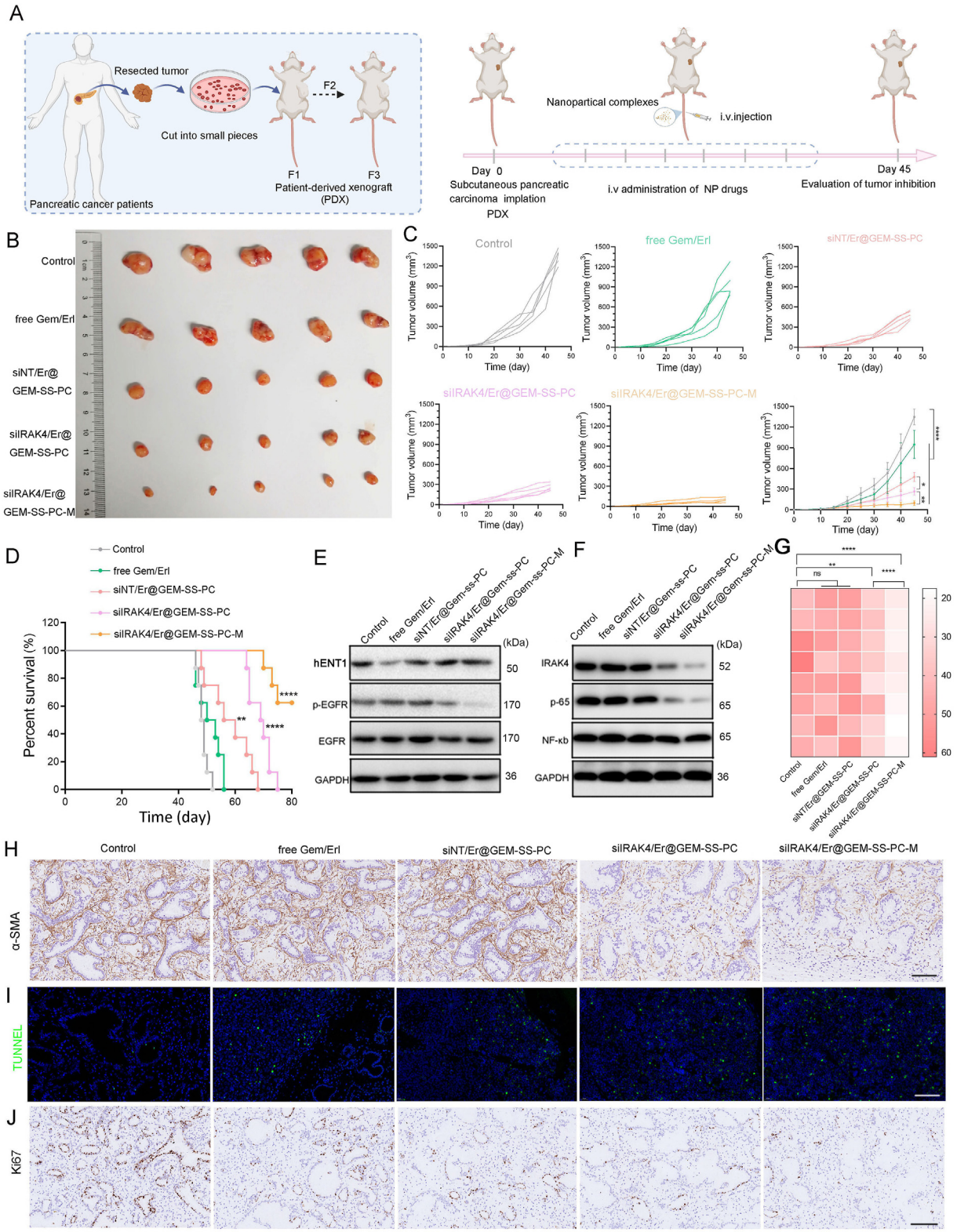

Figure 6 The anti-tumor activity of nano-drug siIRAK4/Er@GEM-SS-PC-M against patient-derived tumor xenograft. (A) Illustration of the therapeutic scheme for the investigation of the antitumor efficacy of nanoparticles against tumor and patient-derived pancreatic tumor. (B) Photograph of excised tumors in different treatment groups on Day 45 ($n = 5$). (C) Tumor growth curves of PDX after being treated by PBS, free GEM and Er, siNT/Er@GEM-SS-PC, siIRAK4/Er@GEM-SS-PC, siIRAK4/Er@GEM-SS-PC-M (mean ± SD, $n = 5$). (D) The survival rate of mice receiving the indicated treatment ($n = 8$, log-rank test). (E) The expression of hENT1 and the phosphorylation of EGFR were determined by Western blot. (F) The expression of IRKA4 and the phosphorylation of p-65 were determined by Western blot. (G) The secretion of IL-1β was determined by Elisa. (H and J) Representative images of α-SMA (H), TUNNEL (I), Ki67 (J) positive areas in tumors. Scale bar = 50 μm.

targeting ability. Furthermore, the survival time of the mice bearing human pancreatic cancer treated with siIRAK4/Er@GEM-SS-PC-M was extremely prolonged among the groups (Fig. 6D). Next, we measured the hENT1 expression and EGFR phosphorylation in tumor tissues by Western blot, and found that the inhibition effects of the combination of free GEM and Er on hENT1was abolished accompanied by the downregulated EGFR phosphorylation level by the nano-drug treatment (Fig. 6E, Supporting Information Fig. S21). Moreover, the expression of IRAK4, the phosphorylation of NF-κB and its downstream cytokine IL-1β was significantly decreased by the siIRAK4/Er@GEM-SS-PC-M treatment (Fig. 6F, G and Fig. S21). An anti-fibrosis response was also observed in the tumor sections of mice that were treated with the siIRAK4/Er@GEM-SS-PC-M and siIRAK4/Er@GEM-SS-PC, which showed an obviously increased α-SMA positive activated fibroblasts compared to the control group (Fig. 6H and Supporting Information Fig. S22). Moreover, the mice that were pretreated with the siIRAK4/Er@GEM-SS-PC-M displayed obvious proliferation inhibition and apoptosis levels in the tumors, as indicated by Ki67$^+$ staining and TUNNEL$^+$ staining, respectively (Fig. 6I, J, and Fig. S22). Finally, no significant loss of body weight, impairment of cardiac function, liver function, renal function, and hematopoiesis were observed in the mice bearing tumors treated with siIRAK4/Er@GEM-SS-PC-M (Supporting Information Figs. S23 and S24), suggesting the excellent biocompatibility and bio-safety of the current nano-drug therapeutic strategy. Together, these results suggest this nano-drug siIRAK4/Er@GEM-SS-PC we have developed is effective for the treatment of pancreatic PDX mode.

4. Conclusions

We have successfully established a new therapeutic strategy that combines chemotherapy, targeted molecular therapy and anti-fibrotic gene therapy for the effective combinational treatment of pancreatic cancer through membrane coated carrier mediated co-delivery of GEM, Er and siIRAK4. The functionalized nano-drug, as expected, could block the antagonism between the GEM and Er as well as modulate the fibrotic microenvironment of pancreatic cancer, and thereby greatly facilitate the anti-pancreatic cancer treatment. It was noted that the nano-drug siIRAK4/Er@GEM-SS-PC-M was independent of nucleoside transporters for entering into the pancreatic cancer cells and exerted superior ability to prevent the cell proliferation and migration. Moreover, the nanosystem-mediated inhibition of IRAK4 suppressed NF-κB-mediated production of pro-fibrotic cytokines IL-1β, and thereby promoted the deep-tissue penetration. Most importantly, the delivery of siIRAK4/Er@GEM-SS-PC-M substantially restrained tumor growth and extended the survival time of mice bearing orthotopic pancreatic tumor and patient-derived tumor. The success of this combinational therapeutic strategy not only defines a unique strategy for effective pancreatic cancer therapy, but also offers considerable promise in the clinical investigations where response rate to GEM and Er in pancreatic cancer patients is currently very limited.

Acknowledgment

The authors acknowledge the National Key Research and Development Program of China (No. 2018YFA0901800), Natural Science Foundation of Zhejiang Province (Distinguished Young Scholar Program, No. LR21H300002, China), National Natural Science Foundation of China (Nos. 81573003 and 32000992), Chinese Society of Clinical Oncology (CSCO) oncology research foundation (Nos. Y-XD2019-243 and Y-Roche2019/2-0042), Joint Foundation of Zhejiang Natural Science Foundation-Zhejiang Society for Mathematical Medicine (LSY19H160005, China) and the Chinese Postdoctoral Science Foundation (2018M642469), Scientific Research Fund of Zhejiang Provincial Education Department (Y202148347, China).

Author contributions

Da Li, Yuan ping and Bowen Li designed the research. Honglin Tang, Bowen Li and Yanan Xue carried out the experiments and performed data analysis. Xiaojie Xu, Fu Zhang, Jiajing Guo and Tingting Yuan participated part of the experiments. Qijun Li, Yuan Chen and Yubin Pan provided experimental drugs and quality control. Honglin Tang and Bowen Li wrote the manuscript. Yuan ping and Da Li revised the manuscript. All of the authors have read and approved the final manuscript.

Conflicts of interest

The authors have no conflicts of interest to declare.

Appendix A. Supporting infomation

Supporting data to this article can be found online at https://doi.org/10.1016/j.apsb.2022.02.007.

References

1. Fan P, Zhao JY, Meng ZB, Wu HY, Wang B, Wu HS, et al. Overexpressed histone acetyltransferase 1 regulates cancer immunity by increasing programmed death-ligand 1 expression in pancreatic cancer. *J Exp Clin Cancer Res* 2019;**38**:47.
2. Mizrahi JD, Surana R, Valle JW, Shroff RT. Pancreatic cancer. *Lancet* 2020;**395**:2008–20.
3. Debernardi S, O'Brien H, Algahmdi AS, Malats N, Stewart GD, Plješa-Ercegovac M, et al. A combination of urinary biomarker panel and PancRISK score for earlier detection of pancreatic cancer: a case-control study. *PLoS Med* 2020;**17**:e1003489.
4. Qin C, Yang G, Yang JS, Ren B, Wang HY, Chen GY, et al. Metabolism of pancreatic cancer: paving the way to better anticancer strategies. *Mol Cancer* 2020;**19**:50.
5. Amrutkar M, Gladhaug IP. Stellate cells aid growth-permissive metabolic reprogramming and promote gemcitabine chemoresistance in pancreatic cancer. *Cancers* 2021;**13**:601.
6. Karasic TB, O'Hara MH, Loaiza-Bonilla A, Reiss KA, Teitelbaum UR, Borazanci E, et al. Effect of gemcitabine and nab-paclitaxel with or without hydroxychloroquine on patients with advanced pancreatic cancer: a phase 2 randomized clinical trial. *JAMA Oncol* 2019;**5**:993–8.
7. Zhang YY, Yang C, Cheng H, Fan ZY, Huang QY, Lu Y, et al. Novel agents for pancreatic ductal adenocarcinoma: emerging therapeutics and future directions. *J Hematol Oncol* 2018;**11**:14.
8. Middleton G, Palmer DH, Greenhalf W, Ghaneh P, Jackson R, Cox T, et al. Vandetanib plus gemcitabine *versus* placebo plus gemcitabine in locally advanced or metastatic pancreatic carcinoma (ViP): a prospective, randomised, double-blind, multicentre phase 2 trial. *Lancet Oncol* 2017;**18**:486–99.

9. Shankar S, Tien JC, Siebenaler RF, Chugh S, Dommeti VL, Zelenka-Wang S, et al. An essential role for argonaute 2 in EGFR−KRAS signaling in pancreatic cancer development. *Nat Commun* 2020;**11**:2817.
10. Li J, Yuan S, Norgard RJ, Yan F, Sun YH, Kim IK, et al. Epigenetic and transcriptional control of the epidermal growth factor receptor regulates the tumor immune microenvironment in pancreatic cancer. *Cancer Discov* 2021;**11**:736−53.
11. Moore MJ, Goldstein D, Hamm J, Figer A, Hecht JR, Gallinger S, et al. Erlotinib plus gemcitabine compared with gemcitabine alone in patients with advanced pancreatic cancer: a phase III trial of the National Cancer Institute of Canada Clinical Trials Group. *J Clin Oncol* 2007;**25**:1960−6.
12. Tempero MA, Malafa MP, Al-Hawary M, Behrman SW, Benson AB, Cardin DB, et al. Pancreatic adenocarcinoma, version 2.2021, NCCN clinical practice guidelines in oncology. *J Natl Compr Cancer Netw* 2021;**19**:439−57.
13. Wei AC, Ou FS, Shi Q, Carrero X, O'Reilly EM, Meyerhardt J, et al. Perioperative gemcitabine + erlotinib plus pancreaticoduodenectomy for resectable pancreatic adenocarcinoma: acosog z5041 (alliance) phase II trial. *Ann Surg Oncol* 2019;**26**:4489−97.
14. Damaraju VL, Scriver T, Mowles D, Kuzma M, Ryan AJ, Cass CE, et al. Erlotinib, gefitinib, and vandetanib inhibit human nucleoside transporters and protect cancer cells from gemcitabine cytotoxicity. *Clin Cancer Res* 2014;**20**:176−86.
15. Sun J, Damaraju VL, Cass CE, Sawyer MB. Inhibition of nucleoside transporters by tyrosine kinase inhibitors and its effects on chemotherapy efficacy. *Cancer Cell Microenviron* 2014;**1**:e389.
16. Miyabayashi K, Ijichi H, Mohri D, Tada M, Yamamoto K, Asaoka Y, et al. Erlotinib prolongs survival in pancreatic cancer by blocking gemcitabine-induced MAPK signals. *Cancer Res* 2013;**73**:2221−34.
17. Damaraju VL, Kuzma M, Mowles D, Cass CE, Sawyer MB. Interactions of multitargeted kinase inhibitors and nucleoside drugs: achilles heel of combination therapy?. *Mol Cancer Therapeut* 2015;**14**:236−45.
18. Li MY, Li HQ, Cheng XL, Wang XP, Li L, Zhou TY, et al. Preclinical pharmacokinetic/pharmacodynamic models to predict schedule-dependent interaction between erlotinib and gemcitabine. *Pharm Res (N Y)* 2013;**30**:1400−8.
19. Semrad T, Barzi A, Lenz HJ, Hutchins IM, Kim EJ, Gong IY, et al. Pharmacodynamic separation of gemcitabine and erlotinib in locally advanced or metastatic pancreatic cancer: therapeutic and biomarker results. *Int J Clin Oncol* 2015;**20**:518−24.
20. Ramakrishnan P, Loh WM, Gopinath CBS, Bonam SR, Fareez IM, Guad RM, et al. Elective phytochemicals targeting pancreatic stellate cells as new anti-fibrotic agents for chronic pancreatitis and pancreatic cancer. *Acta Pharm Sin B* 2020;**10**:399−413.
21. Sato N, Cheng XB, Kohi S, Koga A, Hirata K. Targeting hyaluronan for the treatment of pancreatic ductal adenocarcinoma. *Acta Pharm Sin B* 2016;**6**:101−5.
22. Rossi Sebastiano M, Pozzato C, Saliakoura M, Yang Z, Peng RW, Galiè M, et al. ACSL3-PAI-1 signaling axis mediates tumor-stroma cross-talk promoting pancreatic cancer progression. *Sci Adv* 2020;**6**:eabb9200.
23. Yeung TL, Leung CS, Yip KP, Sheng J, Vien L, Bover LC, et al. Anticancer immunotherapy by MFAP5 blockade inhibits fibrosis and enhances chemosensitivity in ovarian and pancreatic cancer. *Clin Cancer Res* 2019;**25**:6417−28.
24. Hessmann E, Buchholz SM, Demir IE, Singh SK, Gress TM, Ellenrieder V, et al. Microenvironmental determinants of pancreatic cancer. *Physiol Rev* 2020;**100**:1707−51.
25. Dong X, Liu HJ, Feng HY, Yang SC, Liu XL, Lai X, et al. Enhanced drug delivery by nanoscale integration of a nitric oxide donor to induce tumor collagen depletion. *Nano Lett* 2019;**19**:997−1008.
26. Han X, Xu Y, Geranpayehvaghei M, Anderson GJ, Li Y, Nie G. Emerging nanomedicines for anti-stromal therapy against desmoplastic tumors. *Biomaterials* 2020;**232**:119745.
27. Liang C, Shi S, Meng QC, Liang DK, Ji SR, Zhang B, et al. Do anti-stroma therapies improve extrinsic resistance to increase the efficacy of gemcitabine in pancreatic cancer?. *Cell Mol Life Sci* 2018;**75**:1001−12.
28. Valkenburg KC, de Groot AE, Pienta KJ. Targeting the tumour stroma to improve cancer therapy. *Nat Rev Clin Oncol* 2018;**15**:366−81.
29. Kota J, Hancock J, Kwon J, Korc M. Pancreatic cancer: stroma and its current and emerging targeted therapies. *Cancer Lett* 2017;**391**:38−49.
30. Pereira BA, Vennin C, Papanicolaou M, Chambers CR, Herrmann D, Morton JP, et al. CAF subpopulations: a new reservoir of stromal targets in pancreatic cancer. *Trends Cancer* 2019;**5**:724−41.
31. Zhang DX, Li L, Jiang HM, Li Q, Wang-Gillam A, Yu JS, et al. Tumor-stroma IL1β−IRAK4 feedforward circuitry drives tumor fibrosis, chemoresistance, and poor prognosis in pancreatic cancer. *Cancer Res* 2018;**78**:1700−12.
32. Zhang DX, Li L, Jiang HM, Knolhoff BL, Lockhart AC, Wang-Gillam A, et al. Constitutive IRAK4 activation underlies poor prognosis and chemoresistance in pancreatic ductal adenocarcinoma. *Clin Cancer Res* 2017;**23**:1748−59.
33. Fang RH, Hu CM, Luk BT, Gao W, Copp JA, Tai Y, et al. Cancer cell membrane-coated nanoparticles for anticancer vaccination and drug delivery. *Nano Lett* 2014;**14**:2181−8.
34. Hu CM, Fang RH, Luk BT, Zhang L. Polymeric nanotherapeutics: clinical development and advances in stealth functionalization strategies. *Nanoscale* 2014;**6**:65−75.
35. Li RX, He YW, Zhu Y, Jiang LX, Zhang SY, Qin J, et al. Route to rheumatoid arthritis by macrophage-derived microvesicle-coated nanoparticles. *Nano Lett* 2019;**19**:124−34.
36. Ji B, Cai HQ, Yang Y, Peng FH, Song MY, Sun KJ, et al. Hybrid membrane camouflaged copper sulfide nanoparticles for photothermal-chemotherapy of hepatocellular carcinoma. *Acta Biomater* 2020;**111**:363−72.
37. Li D, Li YB, Xing HB, Guo JL, Ping Y, Tang GP. Synergistic enhancement of lung cancer therapy through nanocarrier-mediated sequential delivery of superantigen and tyrosin kinase inhibitor. *Adv Funct Mater* 2014;**24**:5482−92.
38. Chen X, Chen YY, Xin HH, Wan T, Ping Y. Near-infrared optogenetic engineering of photothermal nanoCRISPR for programmable genome editing. *Proc Natl Acad Sci USA* 2020;**117**:2395−405.
39. Tang HL, Xu XJ, Chen YY, Xin HH, Wan T, Li BW, et al. Reprogramming the tumor microenvironment through second-near-infrared-window photothermal genome editing of PD-L1 mediated by supramolecular gold nanorods for enhanced cancer immunotherapy. *Adv Mater* 2021;**33**:e2006003.
40. Varan G, Akkın S, Demirtürk N, Benito JM, Bilensoy E. Erlotinib entrapped in cholesterol-depleting cyclodextrin nanoparticles shows improved antitumoral efficacy in 3D spheroid tumors of the lung and the liver. *J Drug Target* 2021;**29**:439−53.
41. Tóth G, Jánoska Á, Szabó Z, Völgyi G, Orgován G, Szente L, et al. Physicochemical characterisation and cyclodextrin complexation of erlotinib. *Supramol Chem* 2016;**28**:656−64.
42. Fass D, Thorpe C. Chemistry and enzymology of disulfide cross-linking in proteins. *Chem Rev* 2018;**118**:1169−98.
43. Bawa KK, Oh JK. Stimulus-responsive degradable polylactide-based block copolymer nanoassemblies for controlled/enhanced drug delivery. *Mol Pharm* 2017;**14**:2460−74.
44. Lee MH, Yang ZG, Lim CW, Lee YH, Dongbang S, Kang CH, et al. Disulfide-cleavage-triggered chemosensors and their biological applications. *Chem Rev* 2013;**113**:5071−109.
45. Felber JG, Zeisel L, Poczka L, Scholzen K, Busker S, Maier MS, et al. Selective, modular probes for thioredoxins enabled by rational tuning of a unique disulfide structure motif. *J Am Chem Soc* 2021;**143**:8791−803.
46. Tanaka H, Takahashi T, Konishi M, Takata N, Gomi M, Shirane D, et al. Self-degradable lipid-like materials based on "hydrolysis accelerated by the intra-particle enrichment of reactant (hyper)" for messenger RNA delivery. *Adv Funct Mater* 2020;**30**:1910575.
47. Zhou Z, Wang XW, Zhang H, Huang HX, Sun LN, Ma L, et al. Activating layered metal oxide nanomaterials *via* structural

engineering as biodegradable nanoagents for photothermal cancer therapy. *Small* 2021;**17**:e2007486.
48. Yu GC, Zhu BY, Shao L, Zhou J, Saha ML, Shi BB, et al. Host–guest complexation-mediated codelivery of anticancer drug and photosensitizer for cancer photochemotherapy. *Proc Natl Acad Sci U S A* 2019; **116**:6618−23.
49. Cheng W, Zeng XW, Chen HZ, Li ZM, Zeng WF, Mei L, et al. Versatile polydopamine platforms: synthesis and promising applications for surface modification and advanced nanomedicine. *ACS Nano* 2019; **13**:8537−65.
50. Sun BJ, Luo C, Zhang XB, Guo MR, Sun MC, Yu H, et al. Probing the impact of sulfur/selenium/carbon linkages on prodrug nanoassemblies for cancer therapy. *Nat Commun* 2019;**10**:3211.
51. Chen D, Zhu XF, Tao WR, Kong Y, Huag Y, Zhang YJ, et al. Regulation of pancreatic cancer microenvironment by an intelligent gemcitabine@nanogel system *via in vitro* 3D model for promoting therapeutic efficiency. *J Control Release* 2020;**10**:545−59.
52. Fujita M, Somasundaram V, Basudhar D, Cheng RYS, Ridnour LA, Higuchi H, et al. Role of nitric oxide in pancreatic cancer cells exhibiting the invasive phenotype. *Redox Biol* 2019;**22**:101158.